ISSN 1810-2328, Journal of Engineering Thermophysics, 2023, Vol. 32, No. 1, pp. 89–99. © Pleiades Publishing, Ltd., 2023.

# Effects of Slip, Porosity and Chemical Reaction over a Curved Stretching Surface with Mass Transfer

**M. Naveed[1*], Z. Abbas[2], and M. Sajid[3]**

[1]*Department of Mathematics, Division of Science and Technology, University of Education, Lahore, Pakistan*

[2]*Department of Mathematics, The Islamia University of Bahawalpur, Bahawalpur, Pakistan*

[3]*Department of Mathematics and Statistics, International Islamic University, Islamabad, Pakistan*

Received March 4, 2020; in final form, December 18, 2022; accepted January 9, 2023

**Abstract**—This paper presents the effects of wall slip and mass transfer on a viscous fluid over a curved stretching sheet through a Darcian porous medium in the presence of first order chemical reaction. The obtained governing differential equations in a curvilinear coordinate system are transformed into a set of nonlinear ordinary differential equations. The numerical solution for the governing nonlinear boundary value problem is obtained by shooting method with Runge–Kutta integration scheme. The influences of various physical parameters on the fluid velocity and concentration field are shown graphically and analyzed in detail. Numerical results for local skin friction coefficient and local Sherwood number are tabulated for different values of involved parameter.

**DOI:** 10.1134/S1810232823010083

## 1. INTRODUCTION

The mechanism of mass, heat and momentum transfer occurs in many engineering processes when a viscous fluid is flowing past a stretching sheet. The examples of such engineering processes included polymer engineering, electro chemistry, extrusion of plastic sheet, glass fiber production, the cooling and drying of paper and textiles along thread travelling between a feed roll and a wind-up roll, transpiration cooling, packed bed chemical reactors and continues filament extrusion from a dye. Due to a wide range of applications in science and technology, the study of mass transfer in the presence of chemical reaction is of great interested to engineers and scientist. First, Sakiadis [1] studied the boundary layer flow over a continues solid surface moving with a constant speed. The problem of boundary layer viscous flow considered by Sakiadis is extended for a stretching boundary by Crane [2]. He is lucky enough to obtain a closed form solution of the problem. Later, Macleod and Rajagopal [3] discussed the existence and uniqueness of the Crane's problem. Gupta and Gupta [4] studied the heat and mass transfer on a stretching surface with suction or blowing. Chakrabarti and Gupta [5] extended the stretching flow problem by incorporating heat and mass transfer effects. The applications of this problem in electrochemistry has been discussed by Gorla [6]. Chen and Char [7] discussed the analysis of heat transfer over a continuous stretching surface in the presence of suction or blowing. The transport mechanism of chemically reactive species has been investigated by Anderson et al. [8]. Ali [9] investigated the thermal boundary-layer on a power-law stretching surface with suction or injection. More recently, Takhar [10] and Akyildz et al. [11] respectively analyzed the mass transfer effects in the viscous and non-Newtonian fluid. Flow and heat transfer over a stretching sheet when the fluid is passing through a porous medium has been discussed by Vajravelu [12]. In all above studies a no-slip boundary condition is imposed at the solid boundary. The analysis for a partial slip flow is considered by Wang [13]. He obtained a numerical solution of the problem. Kandasamy et al. [14] presented the analysis to obtain the non-linear MHD flow with heat and mass transfer characteristics of an electrically conducting viscous fluid on a vertical stretching sheet with chemical

[*]Corresponding author. E-mail: rana.m.naveed@gmail.com

reaction and thermal stratification effects. Recently Pal and Mondal [15] discussed the effects of Soret-Dufour, chemical reaction on MHD non-Darcian mixed convective heat and mass transfer past a non-linear stretching sheet numerically. In another paper, Pal and Mondel [16] discussed the combined effects of Soret and Dufour on mixed convection past a stretching sheet embedded in a saturated porous medium in the presence of thermal radiation and first order chemical reaction. Bhattacharyya [17] presented the dual nature of solutions in boundary layer stagnation-point flow and mass transfer with chemical reaction over a stretching/shrinking sheet. Subhashini et al. [18] investigated the dual solutions in a double-diffusive convection near stagnation-point region over a stretching vertical sheet with constant wall temperature. Kameswaran et al. [19] studied the hydromagnetic nanofluid flow due to a stretching/shrinking sheet with viscous dissipation in the presence of chemical reaction.

A literature survey indicate that abundant amount of work has been done for the stretching flow problems when the stretching sheet is flat. In such a situation a Cartesian coordinate system is used to model the flow problem. However, the literature is scarce for the flow phenomena over a curved stretching surface. Recently, Sajid et al. [20] initiated to study the boundary layer flow of viscous fluid over a curved stretching surface. They used the curvilinear coordinate system to model the boundary layer equations and obtained a similarity solution numerically using a shooting algorithm with Rung–Kutta integration scheme. In another paper Sajid et al. [21] investigated flow of a micropolar fluid over a curved stretching surface. The effects of partial slip through porous medium in a curved stretching sheet for a micropolar fluid has been discussed by Sajid and Iqbal [22]. Naveed et al. [23–24] also used such curvilinear coordinates for discussing the nanofluid flows for the curved moving geometries.

The aim of this investigation is to study the boundary layer flow and mass transfer over a curved stretching sheet through a porous medium by taking into account of slip effects and first order chemical reaction. It is also assumed that the stretching velocity and surface concentration vary linearly with distance. The obtained set of governing equations in dimensionless form is solved numerically by using a shooting technique with Runge–Kutta integration scheme. The numerical results are depicted graphically and discussed for various physical parameters. The paper is organized as follows: Mathematical formulation is presented in Section 2. Section 3 contains the numerical results and their discussion. The conclusion is summarized in Section 4.

## 2. MATHEMATICAL FORMULATION

Consider the steady, two-dimensional boundary layer flow of an incompressible viscous fluid in a porous medium over a curved stretching sheet coiled in a circle of radius $R$ (as shown in Fig. 1). The mass transfer is the flow along the sheet that contains a species $A$ slightly soluble in a fluid $B$. Let $c_w$ be the concentration at the sheet and the solubility of $A$ in $B$, and concentration of $A$ far away from the sheet is $c_\infty$. It is also assumed that the reaction species $A$ with $B$be the first-order homogenous chemical reaction of the rate constant $k_1$. The concentration of $A$ is assumed to be small enough. The continuity, momentum and mass transfer equations after applying boundary layer approximations are given as:

$$\frac{\partial}{\partial r}\left\{(r+R)\,v\right\}+R\frac{\partial u}{\partial s}=0, \tag{1}$$

$$\frac{u^2}{r+R}=\frac{1}{\rho}\frac{\partial p}{\partial r}, \tag{2}$$

$$\begin{aligned} v\tfrac{\partial u}{\partial r}+\frac{Ru}{r+R}\frac{\partial u}{\partial s}+\frac{uv}{r+R}&=-\frac{1}{\rho}\frac{R}{r+R}\frac{\partial p}{\partial s}\\ &+\nu\left(\frac{\partial^2 u}{\partial r^2}+\frac{1}{r+R}\frac{\partial u}{\partial r}-\frac{u}{(r+R)^2}\right)-\tfrac{\varphi_1 u}{k_1}, \end{aligned} \tag{3}$$

$$v\frac{\partial c}{\partial r}+\frac{Ru}{r+R}\frac{\partial c}{\partial s}=D\left(\frac{\partial^2 c}{\partial r^2}+\frac{1}{r+R}\frac{\partial c}{\partial r}\right)-k_2c, \tag{4}$$

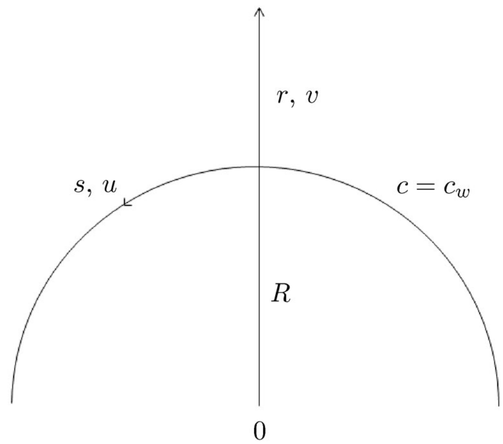


**Fig. 1.** Geometry of the flow problem.

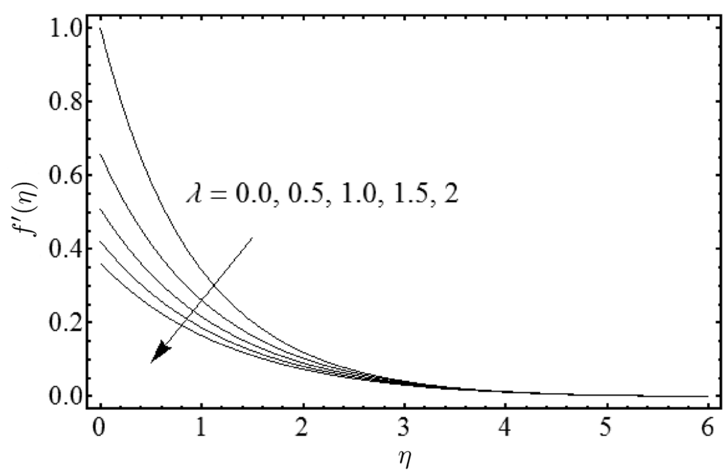


**Fig. 2.** Variation in $f'(\eta)$ for several values of $\lambda$ with $K = 10$ and $D_a = 0.2$.

**Table 1.** Comparison of the numerical values of skin friction coefficient $-\mathrm{Re}_s^{1/2} C_f$ with previously published data with $D_a = 0$ and $K \to \infty$ (i.e., $K = 1000$) fixed

| $\lambda$ | 0.0 | 0.5 | 1.0 | 3.0 | 10 |
|---|---|---|---|---|---|
| Wang [26] | 1.1737 | 06505 | 0.4625 | 0.2231 | 0.0829 |
| Present results | 1.1737 | 06505 | 0.4625 | 0.2231 | 0.0829 |

where $v$ and $u$ are the velocity components in $r$ and $s$ directions, respectively, $\rho$ the fluid density, $p$ the pressure, $\nu$ the kinematics viscosity of fluid, $\mu$ the dynamic viscosity, $k_1$ the permeability of the porous medium, $\varphi_1$ the porosity of a porous medium, $D$ the diffusion coefficient of the diffusing species in the fluid and $c$ the concentration of the species of the fluid.

The appropriate boundary conditions for the problem under consideration are

$$\begin{gathered} u = as + L\left(\frac{\partial u}{\partial r} - \frac{u}{r+R}\right), \quad v = 0, \quad c = c_w \text{ at } r = 0, \\ u \to 0, \quad \frac{\partial u}{\partial r} \to 0, \quad c \to c_\infty \text{ as } r \to \infty, \end{gathered} \tag{5}$$

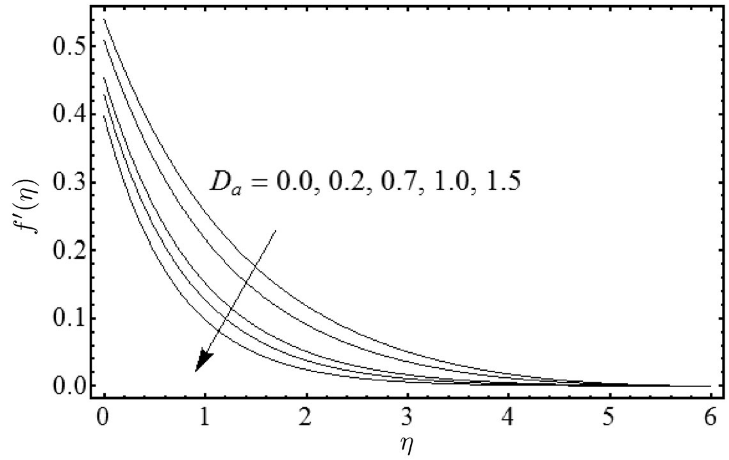


**Fig. 3.** Variation in $f'(\eta)$ for several values of $D_a$ with $K = 10$ and $\lambda = 0.2$.

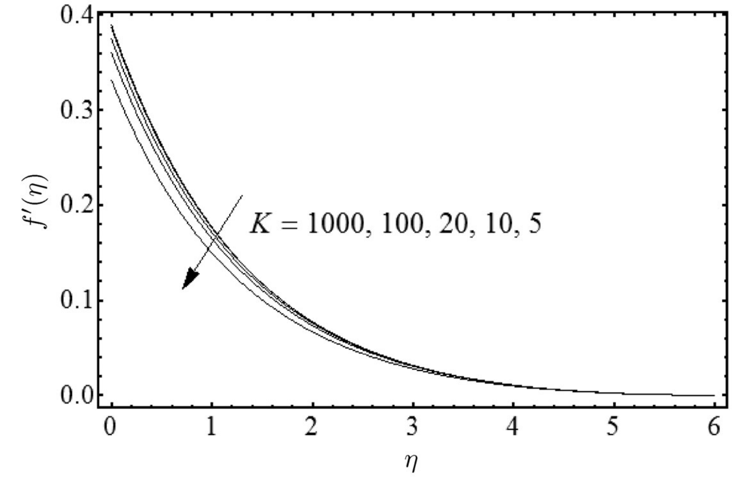


**Fig. 4.** Variation in $f'(\eta)$ for several values of $K$ with $D_a = 0.2$ and $\lambda = 2$.

where $a$ is the stretching constant and has the dimension $(\text{time})^{-1}$ and $L$ the slip length. The no-slip condition can be obtained for $L = 0$.

Invoking the similarity variables

$$\begin{aligned} &u = asf'(\eta), \quad v = \frac{-R}{r+R}\sqrt{a\nu}f(\eta), \quad \eta = \sqrt{\frac{a}{\nu}}r, \\ &p = \rho a^2 s^2 P(\eta), \quad \varphi(\eta) = \frac{c - c_\infty}{c_w - c_\infty}. \end{aligned} \tag{6}$$

Using Eq. (6), Eq. (1) is identically satisfied and Eqs. (2)–(5) yield

$$\frac{\partial P}{\partial \eta} = \frac{f'^2}{\eta + K}, \tag{7}$$

$$\begin{aligned} \frac{2K}{\eta+K}P = f''' + \frac{f''}{\eta+K} - \frac{f'}{(\eta+K)^2} - \frac{K}{\eta+K}f'^2 \\ + \frac{K}{\eta+K}ff'' + \frac{K}{(\eta+K)^2}ff' - D_a f', \end{aligned} \tag{8}$$

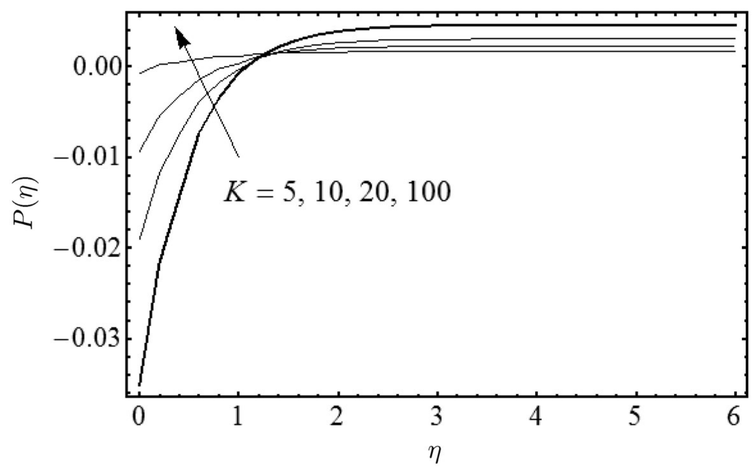


**Fig. 5.** Variation in $P(\eta)$ for several values of $K$ with $D_a = 0.2$ and $\lambda = 0.5$.

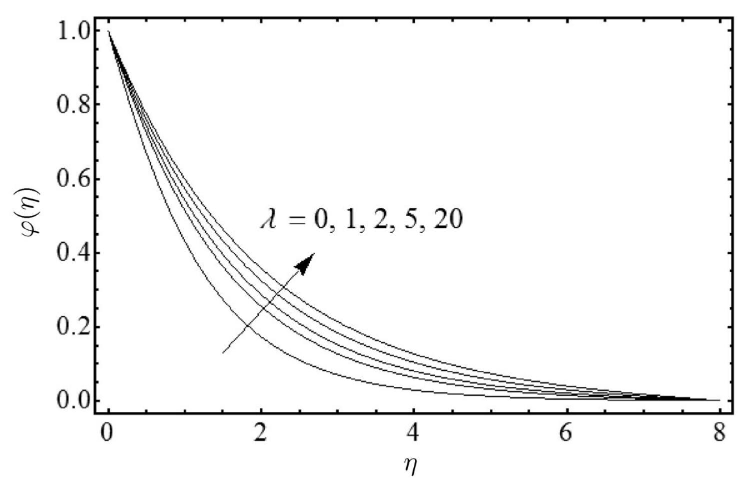


**Fig. 6.** Variation in concentration profile $\varphi(\eta)$ for several values of $\lambda$ with $K = 10$, $Da = 0.5$, $\gamma = 0.2$, and $Sc = 1.0$.

$$\varphi'' + \frac{\varphi'}{\eta + K} + \frac{ScK}{\eta + K} f\varphi' - Sc\beta\varphi = 0, \tag{9}$$

$$\begin{aligned} &f(0) = 0,\ \ f'(0) = 1 + \lambda\left[f''(0) - \frac{f'(0)}{K}\right],\ \ \varphi(0) = 1, \\ &f'(\infty) = 0,\ \ f''(\infty) = 0,\ \ \varphi(\infty) = 0, \end{aligned} \tag{10}$$

where $K = R\sqrt{a/v}$ is the dimensionless radius of curvature, $D_a = \nu\varphi_1/ak_1$ the porosity parameter, $Sc = \nu/D$ the Schmidt number, $\beta = k_2/\alpha$ the chemical reaction parameter and $\lambda = L\,(a/\nu)^{1/2}$ the velocity slip parameter.

Eliminating pressure between Eqs. (7) and (8) results in

$$\begin{aligned} &f^{iv} + \frac{2f'''}{\eta + K} - \frac{f''}{(\eta + K)^2} + \frac{f'}{(\eta + K)^3} - \frac{K}{\eta + K}\left(f'f'' - ff'''\right) \\ &- \frac{K}{(\eta + K)^2}\left(f'^2 - ff''\right) - \frac{K}{(\eta + K)^3} ff' - D_a f'' - D_a \frac{f'}{\eta + K} = 0. \end{aligned} \tag{11}$$

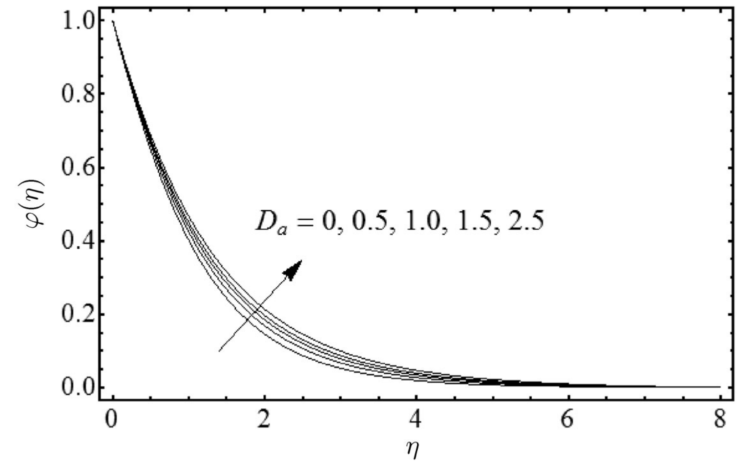


**Fig. 7.** Variation in concentration profile $\varphi(\eta)$ for several values of $D_a$ with $K = 10$, $\lambda = 0.2$, $\gamma = 0.2$, and $Sc = 1.0$.

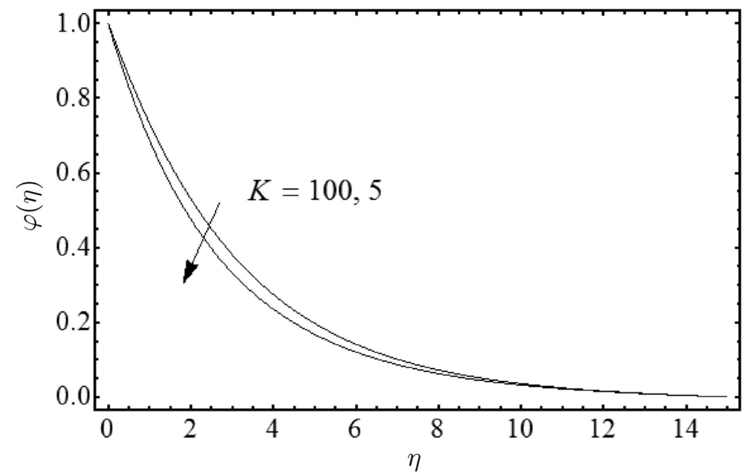


**Fig. 8.** Variation in concentration profile $\varphi(\eta)$ for two values of $K$ with $\lambda = 0.5$, $\gamma = 0.3$, $D_a = 0.2$, and $Sc = 0.2$.

Once we obtain the fluid velocity profile $f(\eta)$, the pressure can be determined from Eq. (8) as follows

$$P(\eta) = \frac{\eta + K}{2K}\left[\begin{array}{l} f''' + \dfrac{f''}{\eta + K} - \dfrac{f'}{(\eta + K)^2} - \dfrac{K}{\eta + K} f'^2 \\ + \dfrac{K}{\eta + K} f f'' + \dfrac{K}{(\eta + K)^2} f f' - D_a f' \end{array}\right]. \tag{12}$$

The physical quantities of interest are the skin friction coefficient and the rate of mass transfer at the wall (local Sherwood number) along the $s$-directions, which are defined as

$$C_f = \frac{\tau_{rs}}{\rho u_w^2}, \quad Sh_s = \frac{s j_w}{D(c_w - c_\infty)}, \tag{13}$$

where $\tau_{rs}$ is the wall shear stress and $j_w$ the mass flux at the wall along the $s$-direction, which are given by

$$\tau_{rs} = \mu\left(\frac{\partial u}{\partial r} - \frac{u}{(r + R)}\right)\bigg|_{r=0}, \quad j_w = -D\left.\frac{\partial c}{\partial r}\right|_{r=0}. \tag{14}$$

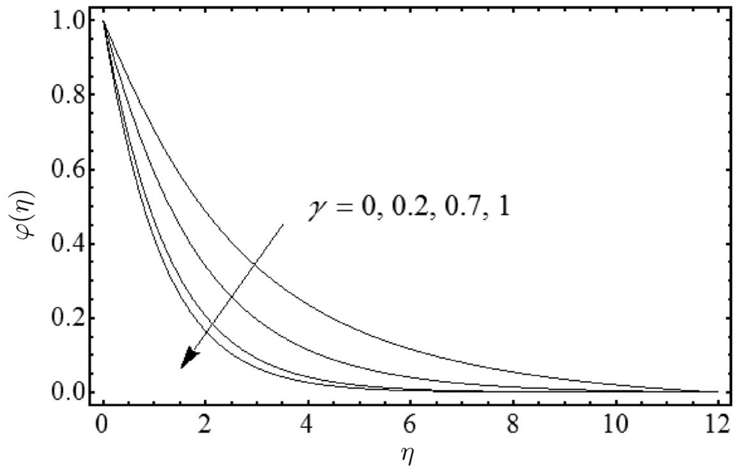


**Fig. 9.** Variation in concentration profile $\varphi(\eta)$ for several values of $\gamma$ with $\lambda = 0.2$, $K = 10$, $D_a = 0.2$, and $Sc = 0.5$.

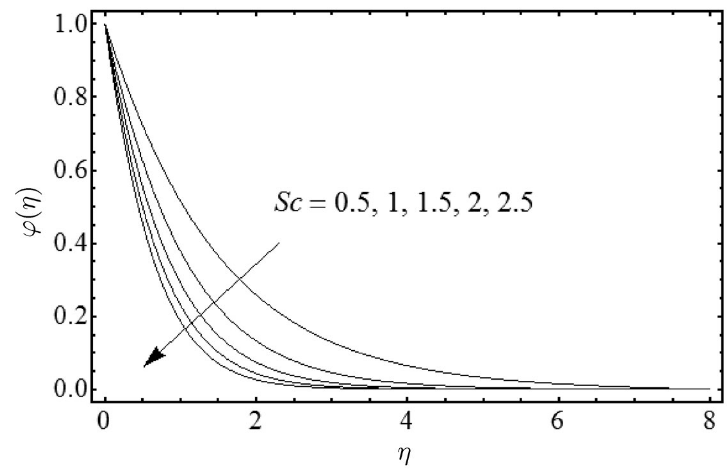


**Fig. 10.** Variation in concentration profile $\varphi(\eta)$ for several values of $Sc$ with $\lambda = 0.2$, $K = 10$, $D_a = 0.2$, and $\gamma = 0.5$.

Using Eq. (6) and Eq. (13) with the help of Eq. (14) becomes

$$\begin{gathered}\mathrm{Re}_s^{1/2} C_f = \left[ f''(0) - \frac{f'(0)}{K} \right], \\ \mathrm{Re}_s^{-1/2} Sh_s = -\varphi'(0), \end{gathered} \tag{15}$$

where $\mathrm{Re}_s = as^2/\nu_f$ is the local Reynold number.

## 3. RESULTS AND DISCUSSION

We compute the velocity and concentration profiles by solving Eqs. (9) and (11) with boundary conditions (10) numerically using a shooting method with Runge–Kutta integration scheme of order four [25]. The velocity field $f'(\eta)$ and the concentration field $\varphi(\eta)$ are plotted to see the influence of various emerging parameters, for example, the velocity slip parameter $\lambda$, the porosity parameter $D_a$, the dimensionless radius of curvature $K$, the Schmidt number $Sc$ and chemical reaction parameter $\gamma$. Furthermore, we compute the numerical values of the skin friction coefficient $-\mathrm{Re}_s^{1/2} C_f$ and the Sherwood number $\mathrm{Re}_s^{-1/2} Sh_s$ for different physical parameters in tabular form.

**Table 2.** Numerical values of skin friction coefficient $-\mathrm{Re}_s^{1/2}C_f$ for different values of $K$, $D_a$, and $\lambda$

| $K$ | $D_a$ | $\lambda=0$ | $\lambda=0.5$ | $\lambda=1$ |
|---|---|---|---|---|
| 5 | 0.5 | 1.4477 | 0.7882 | 0.5531 |
| 10 | | 1.3314 | 0.7428 | 0.5269 |
| 20 | | 1.2773 | 0.7208 | 0.5139 |
| 50 | | 1.2462 | 0.7079 | 0.5061 |
| 100 | | 1.2361 | 0.7036 | 0.5035 |
| 200 | | 1.2311 | 0.7015 | 0.5022 |
| 1000 | | 1.2271 | 0.69988 | 0.5012 |
| 10 | 0 | 1.0874 | 0.6342 | 0.4595 |
| | 0.2 | 1.1921 | 0.6830 | 0.4906 |
| | 0.6 | 1.3741 | 0.7601 | 0.5371 |
| | 0.8 | 1.4552 | 0.7917 | 0.5551 |
| | 1.0 | 1.5314 | 0.8199 | 0.5708 |
| | 1.5 | 1.7049 | 0.8793 | 0.6026 |
| | 2.0 | 1.8603 | 0.9276 | 0.6271 |

Figure 2 shows the effects of velocity slip parameter $\lambda$on the fluid velocity $f'(\eta)$ by keeping $K=10$ and $D_a=0.2$ are fixed. It is observed from Fig. 2 that both the fluid velocity $f'(\eta)$ and the momentum boundary layer thickness are decreased with an increased in $\lambda$. It is also seen that for increased slip parameter $\lambda$ the lateral velocity decreases near the surface but increases at large distance. However, the decrease in fluid velocity at the surface is revealed the flow of fluid comes from stretching of the sheet, therefore any increase in slip of fluid on the stretching sheet causes decrease in fluid velocity profile. It is also observed that with an increase in velocity slip parameter$\lambda$the momentum boundary layer thickness is decreased.

Figure 3 gives the variation in the fluid velocity $f'(\eta)$ for different values of porosity parameter $D_a$ when $K=10$ and $\lambda=1$ are fixed. The velocity profile $f'(\eta)$ decreases by an increasing values of porosity parameter $D_a$, the momentum boundary layer thickness is also decreased as $D_a$ increases. Moreover, the presence of pores in the medium controls the boundary layer thickness.

Figure 4 shows the effects of dimensionless radius of curvature $K$ on the velocity field $f'(\eta)$ with $\lambda=2$ and $D_a=0.2$ fixed. It can be seen from this figure that an increase in the $K$, fluid velocity $f'(\eta)$ and the momentum boundary layer thickness increases. Figure 5 gives the change in pressure distribution $P(\eta)$ for several values of dimensionless radius of curvature $K$ when $\lambda=0.5$ and $D_a=0.2$ are fixed. It is observed that the pressure $P(\eta)$ decreases inside the boundary layer as the dimensionless radius of curvature $K$ increases. Moreover, the pressure goes to zero far away from the boundary, and the magnitude of the pressure approaches to zero by taking $K\to\infty$ (the case in which the curved stretching surface goes to flat stretching surface).

Figure 6 is made to show the variation in concentration field $\varphi(\eta)$ for several values of velocity slip parameter $\lambda$ by keeping all the other parameters fixed. It can be seen that both the concentration of the fluid and the concentration boundary layer thickness are increased with increasing the value of velocity slip parameter $\lambda$. Figure 7 illustrates the concentration field $\varphi(\eta)$ for different values of porosity parameter $D_a$ when $K=10$, $\lambda=0.2$, $\gamma=0.3$, and $Sc=1$ are fixed. It is important to note that an increase in the value of $D_a$ leads to an increase in the concentration of the fluid in concentration boundary layer as seen from this figure.

The variation of concentration profile $\varphi(\eta)$ is depicted in Fig. 8 for two values of dimensionless radius of curvature $K$ when $D_a=0.2$, $\lambda=0.5$, $\gamma=0.3$, and $Sc=0.2$ are fixed. It is found that the

**Table 3.** Numerical values of Sherwood number $\mathrm{Re}_s^{-1/2} Sh_s$ for different values of $K$, $\gamma$, $Sc$, $D_a$, and $\lambda$

| $K$ | $\beta$ | $Sc$ | $D_a$ | $\lambda = 0.5$ | $\lambda = 1$ | $\lambda = 2$ |
|---|---|---|---|---|---|---|
| 5 | 0.2 | 0.5 | 0.5 | 0.4923 | 0.4711 | 0.4506 |
| 10 | | | | 0.4585 | 0.4367 | 0.4149 |
| 20 | | | | 0.4409 | 0.4188 | 0.3963 |
| 50 | | | | 0.4300 | 0.4077 | 0.3848 |
| 100 | | | | 0.4264 | 0.4040 | 0.3808 |
| 1000 | | | | 0.4230 | 0.4006 | 0.3773 |
| 10 | 0.2 | | | 0.4585 | 0.4367 | 0.4149 |
| | 0.4 | | | 0.5754 | 0.5568 | 0.5382 |
| | 0.6 | | | 0.6682 | 0.6514 | 0.6346 |
| | 0.8 | | | 0.7476 | 0.7321 | 0.7165 |
| | 1.0 | | | 0.8183 | 0.8036 | 0.7891 |
| | 1.5 | | | 0.9701 | 0.9571 | 0.9442 |
| | 2.0 | | | 1.0993 | 1.0875 | 1.075 |
| | 0.2 | 0.2 | | 0.2951 | 0.2857 | 0.2762 |
| | | 0.7 | | 0.5467 | 0.5176 | 0.4886 |
| | | 1.0 | | 0.6614 | 0.6224 | 0.5835 |
| | | 1.5 | | 0.8233 | 0.7699 | 0.7166 |
| | | 2.0 | | 0.9621 | 0.8963 | 0.8302 |
| | 0.5 | 0.7 | 0.0 | 0.7599 | 0.7375 | 0.7134 |
| | | | 0.2 | 0.7499 | 0.7269 | 0.7031 |
| | | | 0.6 | 0.7350 | 0.7120 | 0.6895 |
| | | | 0.8 | 0.7292 | 0.7066 | 0.6849 |
| | | | 1.0 | 0.7243 | 0.7020 | 0.6811 |
| | | | 1.5 | 0.7145 | 0.6932 | 0.6741 |
| | | | 2.0 | 0.7071 | 0.6868 | 0.6694 |

concentration of the fluid increases with an increase in $K$. It should also be mentioned that for large values of dimensionless radius of curvature $K$ we found a very small change in the concentration of the fluid. Figure 9 displays the influence of chemical reaction parameter $\gamma$ on the concentration field $\varphi(\eta)$ by keeping $K = 10$, $D_a = 0.2$, $\lambda = 0.2$, and $Sc = 0.5$ are fixed. It is observed from this figure that the chemical reaction decelerates the concentration of the fluid during the slip at the stretching wall as seen from Fig. 9, i.e., increase in the value of the chemical reaction rate parameter shows a sharp decrease in the concentration of the diffusing species. This indicates the fact that concentration of the diffusing species reduces during fast reaction. It is also seen that the concentration boundary layer thickness decreases with increasing the value of $\gamma$.

Figure 10 shows the change in the concentration profile $\varphi(\eta)$ for different values of the Schmidt number $Sc$ when $K = 10$, $D_a = 0.2$, $\lambda = 0.2$, and $\gamma = 0.5$ are fixed. From this figure we found that the effects of the Schmidt number $Sc$ are to decrease both the dimensionless concentration of the fluid $\varphi(\eta)$ and concentration boundary layer thickness with its increase.

The values of the skin friction coefficient $-\mathrm{Re}_s^{1/2}C_f$ is tabulated in Table 1 for various values of dimensionless radius of curvature $K$, porosity parameter $D_a$ and the velocity slip parameter $\lambda$. It is noted that the skin friction coefficient $-\mathrm{Re}_s^{1/2}C_f$ decreases with an increase in the dimensionless radius of curvature in the presence of porosity of a medium and velocity slip parameter, i.e., as the curved stretching changes to the flat stretching sheet by taking $K \to \infty$ and thus decrease the velocity gradient at the wall. It can also be seen that the skin friction coefficient is increased by increasing the values of the porosity parameter $D_a$. This is due to the fact that the presence of the permeability of a porous medium will reduce the velocity of fluid and momentum boundary layer thickness, and increase the shear stress at the wall. On the other hand, the skin friction coefficient $-\mathrm{Re}_s^{1/2}C_f$ at the wall is effectively reduced by the increase of velocity slip parameter $\lambda$.

Table 2 gives the values of the local Sherwood number $\mathrm{Re}_s^{-1/2}Sh_s$ for various values of $K$, $D_a$, $Sc$, $\gamma$, and $\lambda$. It is found that the magnitude of the local Sherwood number decreases with increasing the dimensionless radius of curvature, i.e., as the dimensionless radius of curvature will increase the concentration of the fluid and the concentration boundary layer thickness as seen from Fig. 8 and thus decrease the concentration gradient at the wall. It is also observed that the effects of increasing $D_a$ is to increase the local Sherwood number, whereas the magnitude of the local Sherwood number increases with an increase in $Sc$ and $\gamma$ respectively. On the other hand, the magnitude of the local Sherwood number is decreased with increasing the values of the velocity slip parameter $\lambda$.

## 4. CONCLUDING REMARKS

The problem of steady boundary layer flow of a viscous fluid with mass transfer over a curved stretching sheet in the presence of slip condition and chemical reaction is investigated numerically. The obtained numerical results are presented graphically and in tabular form for various values of dimensionless radius of curvature, slip parameter, porosity parameter, the Schmidt number and chemical reaction parameter. The following observations have been made from this study:

- An increase in slip parameter $\lambda$ at the sheet causes decrease in fluid velocity and momentum boundary layer thickness.
- Both fluid velocity profile and the momentum boundary layer thickness are decreased with an increase in $D_a$.
- The concentration of the fluid increases by increasing the values of velocity slip parameter $\lambda$ and dimensionless radius of curvature $K$.
- The concentration of the fluid is decreased with an increase of $\gamma$ and $Sc$.
- By increasing the value of $\lambda$ both the skin friction coefficient and the local Sherwood number are decreased.

## ACKNOWLEDGMENTS

We are thankful to the honorable reviewers for their encouraging comments and constructive suggestions to improve the quality of the manuscript.

## REFERENCES

1. Sakiadis, B.C., Boundary-Layer Behavior on Continuous Solid Surface, I: Boundary Layer Equations for Two-Dimensional and Axisymmetric Flow, *AIChE J.*, 1961, vol. 7, p. 26.
2. Crane, L.J., Flow past a Stretching Plate, *Z. Angew Math. Mech.*, 1970, vol. 21, pp. 645–647.
3. McLeod, J.B. and Rajagopal, K.R., On the Uniqueness of Flow of a Navier–Stokes Fluid Due to a Stretching Boundary, *Arch. Rat. Mech. An.*, 1987, vol. 98, pp. 385–393.
4. Gupta, P.S. and Gupta, A.S., Heat and Mass Transfer on a Stretching Sheet with Suction and Blowing, *Can. J. Chem. Eng.*, 1977, vol. 55, pp. 744–746.
5. Charkrabarti, A. and Gupta, A.S., Hydromagnetic Flow and Heat Transfer over a Stretching Sheet, *Quart. Appl. Math.*, 1979, vol. 37, p. 73.
6. R.S.R., Unsteady Mass Transfer in the Boundary Layer on a Continuos Moving Sheet Electrode, *J. Electrochem. Soc.*, 1978, vol. 125, pp. 865–869.

7. Chen, C.K. and Char, M.I., Heat Transfer of a Continuous Stretching Surface with Suction and Blowing, *J. Math. An. Appl.*, 1988, vol. 13, pp. 568–580.
8. Andresson, H.I. Hansen, O.R., and Olmedal, B., Diffusion of a Chemically Reactive Species from a Stretching Sheet, *Int. J. Heat Mass Transfer*, 1994, vol. 37, pp. 659–664.
9. Ali, M.E., On Thermal Boundary Layer on a Power Law Stretched Surface with Suction or Injection, *Int. J. Heat Fluid Flow*, 1995, vol. 16, pp. 280–290.
10. Takhar, H.S., Chainkha, A.J., and Nath, G., Flow and Mass Transfer on a Stretching Sheet with a Magnetic Field and Chemically Reactive Species, *Int. J. Eng. Sci.*, 2000, vol. 38, pp. 1303–1314.
11. Akyildiz, F.T, Bellout, H., and Vajravelu, K., Diffusion of Chemically Reactive Species in a Porous Medium over a Stretching Sheet, *J. Math. An. Appl.*, 2006, vol. 320, pp. 322–339.
12. Vajravelu, K., Flow and Heat Transfer in a Saturated Porous Medium over a Stretching Surface, *J. Appl. Math. Mech. (ZAMM)*, 1994, vol. 74, pp. 605–614.
13. Wang, C.Y., Flow Due to a Stretching Boundary with Partial Slip: An Exact Solutions of the Navier–Stokes Equations, *Chem. Eng. Sci.*, 2002, vol. 57, pp. 3745–3747.
14. Kandasamy, R., Periasamy, K., and Sivagnana Prabhu, K.K., Chemical Reaction Heat and Mass Transfer on MHD Flow over a Vertical Stretching Surface with Heat Source and Thermal Stratification Effects, *Int. J. Heat Mass Transfer*, 2005, vol. 48, pp. 4557–4561.
15. Pal, D. and Mondal, H., MHD Non-Darcian Mixed Convection Heat and Mass Transfer over a Non-Linear Stretching Sheet with Soret–Dufour Effects and Chemical Reaction, *Int. Comm. Heat Mass Transfer*, 2011, vol. 38, pp. 463–467.
16. Pal, D. and Mondal, H., Influence of Chemical Reaction and Thermal Radiation on Mixed Convection Heat and Mass Transfer over a Stretching Sheet in Darcian Porous Medium with Soret and Dufour Effects, *Energ. Conv. Mang.*, 2012, vol. 6, pp. 102–108.
17. Bhattacharyya, K., Dual Solutions in Boundary Layer Stagnation-Point Flow and Mass Transfer with Chemical Reaction past a Stretching/Shrinking Sheet, *Int. Comm. Heat Mass Transfer*, 2011, vol. 38, pp. 917–922.
18. Subhashini, S.V., Sumathi,R., and Pop, I., Dual Solutions in a Double-Diffusive Convection near Stagnation Point Region over a Stretching Vertical Surface, *Int. J. Heat Mass Transfer*, 2012, vol. 55, pp. 2524–2530.
19. Kameswaran, P.K., Narayana, M., Sibanda, P., and Murthy, P.V.S.N., Hydromagnetic Nanofluid Flow Due to a Stretching or Shrinking Sheet with Viscous Dissipation and Chemical Reaction Effects, *Int. J. Heat Mass Transfer*, 2012, vol. 55, pp. 7587–7595.
20. Sajid, M., Ali, N., Javed, T., and Abbas, Z., Stretching a Curved Surface in a Viscous Fluid, *Chin. Phy. Lett.*, 2010, vol. 27, p. 024703.
21. Sajid, M., Ali, N., Javed, T., and Abbas, Z., Flow of a Micropolar Fluid over a Curved Stretching Surface, *J. Eng. Phys. Thermophys.*, 2011, vol. 84, pp. 798–804.
22. Sajid, M. and Iqbal, S.A., Stretching a Curved Surface through Porous Medium in a Micropolar Fluid with Partial Slip, *Int. J. Mech. Sys. Eng.*, 2011, vol. 1, pp. 1–7.
23. Naveed, M., Abbas, Z., and Sajid, M., Nonlinear Radiative Heat Transfer in Blasius and Sakiadis Flows over a Curved Surface, *Int. J. Therm. Phys.*, 2017, vol. 38, p. 14.
24. Naveed, M., Abbas, Z., and Sajid, M., Thermophoresis and Brownian Effects on the Blasius Flow of a Nanfluid Due to a Curved Surface with Thermal Radiation, *Eur. Phys. J. Plus*, 2016, vol. 131, p. 214.
25. Na, T.Y., *Computational Methods in Engineering Boundary Value Problems*, New York: Academic Press, 1979.
26. Wang, C.Y., Analysis of Viscous Flow Due to a Stretching Sheet with Surface Slip and Suction, *Nonlin. An. Re. World. Appl.*, 2009, vol. 10, pp. 375–380.